Supplementary for

Effects of sedimentation, microgravity hydrodynamic mixing and air-water interface on α-synuclein amyloid formation

Jiangtao Zhou[1, †], Francesco S. Ruggeri[2, 3, †,], Manuela R, Zimmermann[2], Georg Meisl[2], Giovanni Longo[4], Sergey K. Sekatskii[1], Tuomas P. J. Knowles[2, 3,*] and Giovanni Dietler[1,*]*

1. Laboratory of Physics of Living Matter, École Polytechnique Fédérale de Lausanne (EPFL), CH-1015 Lausanne, Switzerland
2. Department of Chemistry, University of Cambridge, Lensfield Road, Cambridge CB2 1EW, UK
3. Centre for Misfolding Diseases, Department of Chemistry, University of Cambridge, Lensfield Road, Cambridge CB2 1EW, UK
4. Istituto di Struttura della Materia, CNR, Via del Fosso del Cavaliere 100, 00133, Roma, Italy

† These authors contributed equally to this work

*corresponding author: fsr26@cam.ac.uk , tpjk2@cam.ac.uk and giovanni.dietler@epfl.ch

Supplementary Information Text

1. Characterization of the average diameter and volume of amyloid fibrils

The positive functionalized mica employed for AFM analysis is atomically flat with a surface roughness of less than 0.2 nm, and thus it is an ideal substrate to characterize the dimensions and the volume of the negative aggregates of α-synuclein with sub-nanometer resolution. The average height of α-synuclein fibrils was measured as shown in **Figure S1**. The average diameter of the amyloid fibrils was extracted as the average of the maximum of multiple cross-section perpendicular to the fibril axis[1,2].

In each condition, the volume of fibrillar aggregates was also detected on multiple 4×4 μm^2 3-D morphology maps (**Figure S3a**), with a height threshold value of 1 nm to exclude smaller aggregates. Statistical comparison of fibril volume between different conditions (**Figure S3b**) were realized by probing six random locations and comparing the fibril volume captured on the same size of AFM images.

2. Comparison of static conditions in Eppendorf and syringe

The aggregation process under static conditions both in the absence and presence of an air-water interface was similar and significantly slower than that all the other conditions at all measured concentrations. To quantitatively compare the process of aggregation in these two conditions, we measured the volume of fibrillar aggregates formed in each condition. For instance, in **Figure S4**, we show the volume of fibrils formed after 30 days and 54 days of incubation at 45 μM in static condition. The amount of fibrils produced at the different time points was similar, confirming that these two static conditions show no significant difference (**Figures S4**).

3. Aggregation in static and microgravity conditions

In static and microgravity-Syr conditions, protein aggregation was observed to be slower than that in all other conditions and mature fibrils were formed only after 54 days of incubation as observed by AFM (**Figure S2**) imaging and CD (**Figure S7**) spectroscopy.

4. AFM characterization of fibrillar polymorphism

To better appreciate the fibrils obtained from different incubated conditions, the high-resolution AFM images and morphological analysis of the fibrillar aggregates formed under different condition are displayed in **Figure S5-S6**. In static conditions, for both syringe and Eppendorf tube, we observed the abundant formation of twisted fibril polymorphs. In microgravity without any air-water interface, both twisted and rod-like polymorphs were observed. Orbital shaking without an air-water interface induced a homogenous rod-like fibril morphology, whereas orbital shaking in the presence of air-water interface induced amorphous massive fibril bundles as an accumulation of rod-like fibrils. Microgravity in the

presence of the rotating air-water interface lead to the formation of a mixture of parallel-stacked twisted fibrils. This polymorphism indicates that different hydrodynamic mixing and interfacial interactions can play a considerable role in determining the fibrillization mechanism and the pathway of fibril formation.

5. Interpretation of CD spectroscopy and ThT assay

The CD data at the concentration of 45 μM showed that in the case of static (**Figure 3a)** and microgravity-Syr (**Figure 3b**) conditions, the spectra evolution as a function of incubation time showed no significant β-sheet conformation in the first 20 days, although the random coil content clearly decreased. In these conditions, the CD spectra showed only full interconversion of disordered monomeric proteins into ordered cross-β sheet only after 35 days (microgravity-Syr) and 48 days (static) of incubation (**Figure S7**). In agreement with the AFM measurements, the cross-β sheet interconversion was slightly faster in microgravity-Syr conditions than that in static conditions in both the presence and absence of an air-water interface. Incubation in condition of orbital shaking in the absence of an air-water interface showed an intermediate behavior and a full cross-β sheet interconversion after 20 days of incubation. The fastest transition from random coil to cross-β sheet content was observed for the conditions in which a moving air-water interface was present, the Eppendorf tube subjected to microgravity rotation or to orbital shaking. In both cases, the random coil monomeric proteins converted into cross-β sheet structure already after 13 days of incubation.

The ThT data showed that at the concentration of 45 μM (**Figure S8**), α-synuclein aggregation under the Static-Epp conditions reached the dynamic equilibrium (plateau phase) only after 50 days of incubation, while the microgravity conditions in absence of air-water interface after ~40 days. In the OShaking-Syr condition, the plateau phase was observed after 30 days of incubation. In presence of a moving air-water interface, we noticed that the ThT signals under the microgravity-Epp and OShaking-Epp conditions showed a short lag phase and reached the plateau phase after 15-20 days of incubation.

To quantify the tendency of the protein to aggregate in each condition, ThT fluorescence intensity and the CD signal at 220 nm at the same time point were plotted as a function of incubation time (**Figure S9**). The results show similar trends of structural evolution and β-sheet formation in each condition, suggesting the correspondence of the characterization between CD spectroscopy and ThT assay, and indicating the reliability of the characterization of protein aggregation.

6. Further mechanistic investigations

An alternative approach to investigate which microscopic step is most likely affected by a change in the experimental conditions is to describe the observed effects by allowing variation of only one specific microscopic step and then compare which scenario best describes the data. This analysis was also performed

using the online fitting software amylofit, and the general model 'secondary nucleation dominated, unseeded'. To study effects on primary nucleation, the fitting parameters related to primary nucleation, i.e. k_+k_n and n_c, were allowed to vary with the experimental conditions, whereas the remaining fitting parameters were constrained to one global value for all conditions. The rate of primary nucleation, λ, was then calculated as before using

$$\lambda = \sqrt{2\, k_+ k_n m_0^{n_c}}$$

where m_0 indicated the monomer concentration. The effects on secondary processes were studied analogously, i.e. the fitting parameters related to secondary processes, namely k_+k_2 and n_2, were allowed to vary with the experimental conditions, whereas the remaining fitting parameters were constrained to one global value for all conditions. The rate of secondary processes, κ, was then evaluated according to

$$\kappa = \sqrt{2\, k_+ k_2 m_0^{(n_2+1)}}$$

where m_0 denoted again the monomer concentration. Finally, effects on the elongation reaction were studied analogously, but utilizing the model 'secondary nucleation dominated', which allows to decouple the rate constant of elongation, k_+, from the rate constant of primary nucleation or secondary processes respectively. The fitting results are shown in **Figures S12** (primary nucleation), **S13** (secondary processes) and **S14** (elongation). Panel a in these figures shows the variation of the parameter allowed to vary with condition. The mean squared errors obtained when allowing different parameters to vary were comparable, and therefore none of the scenarios could be ruled out, i.e. it could not be determined whether the altered experimental conditions mainly affected primary nucleation, secondary processes or elongation. This indicated that the tested experimental conditions influenced the aggregation of α-synuclein in a more complex manner than just one single process. Indeed, the fits represented the data better when changes in both primary nucleation and secondary processes were allowed (compare fits in **Figures S12**, **S13** and **S14** to those in **Figure S11**). This is not surprising given that this study encompasses the effects of several distinct experimental features. The way in which the tested experimental conditions likely affect primary nucleation and secondary processes is discussed in the main text.

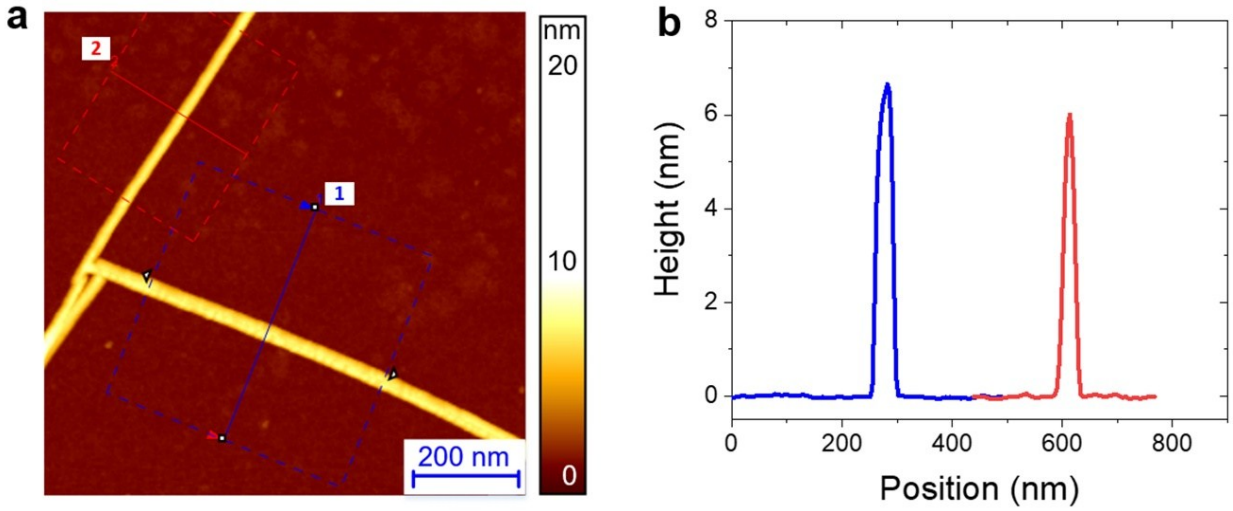

Figure S1| Method of characterization of average fibrillar cross-sectional height. (a) The height of a fibril at the cross-section (solid line) was measured and then averaged along the fibrils in the dashed box. (b) Examples of average cross-sectional heights of fibril 1 (blue) and fibril 2 (red) in the dashed boxes.

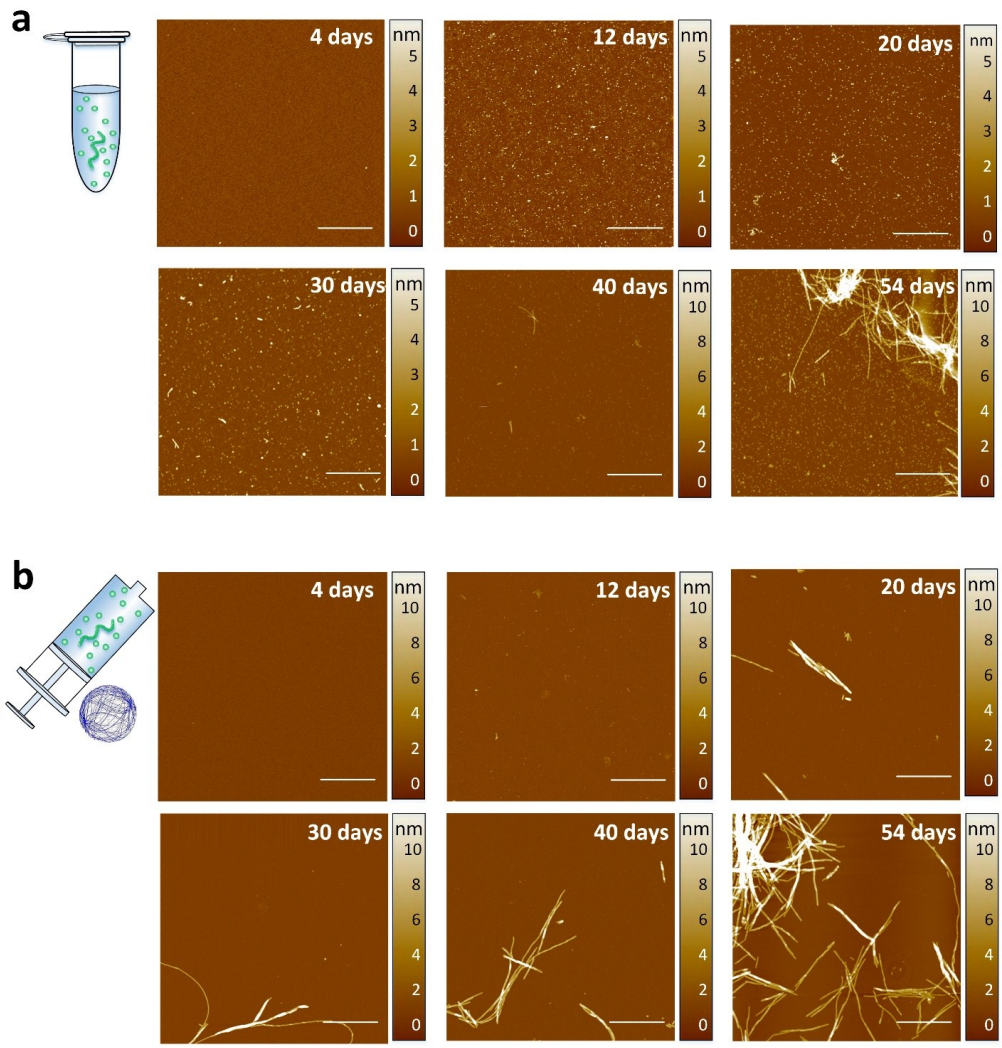

Figure S2| Fibril formation process in static Eppendorf and microgravity syringe conditions. Morphology of α-Synuclein aggregates after 4, 8, 12, 16, 20, 30, 40, and 54 days of incubation in static Eppendorf (a) and microgravity syringes (b) conditions.

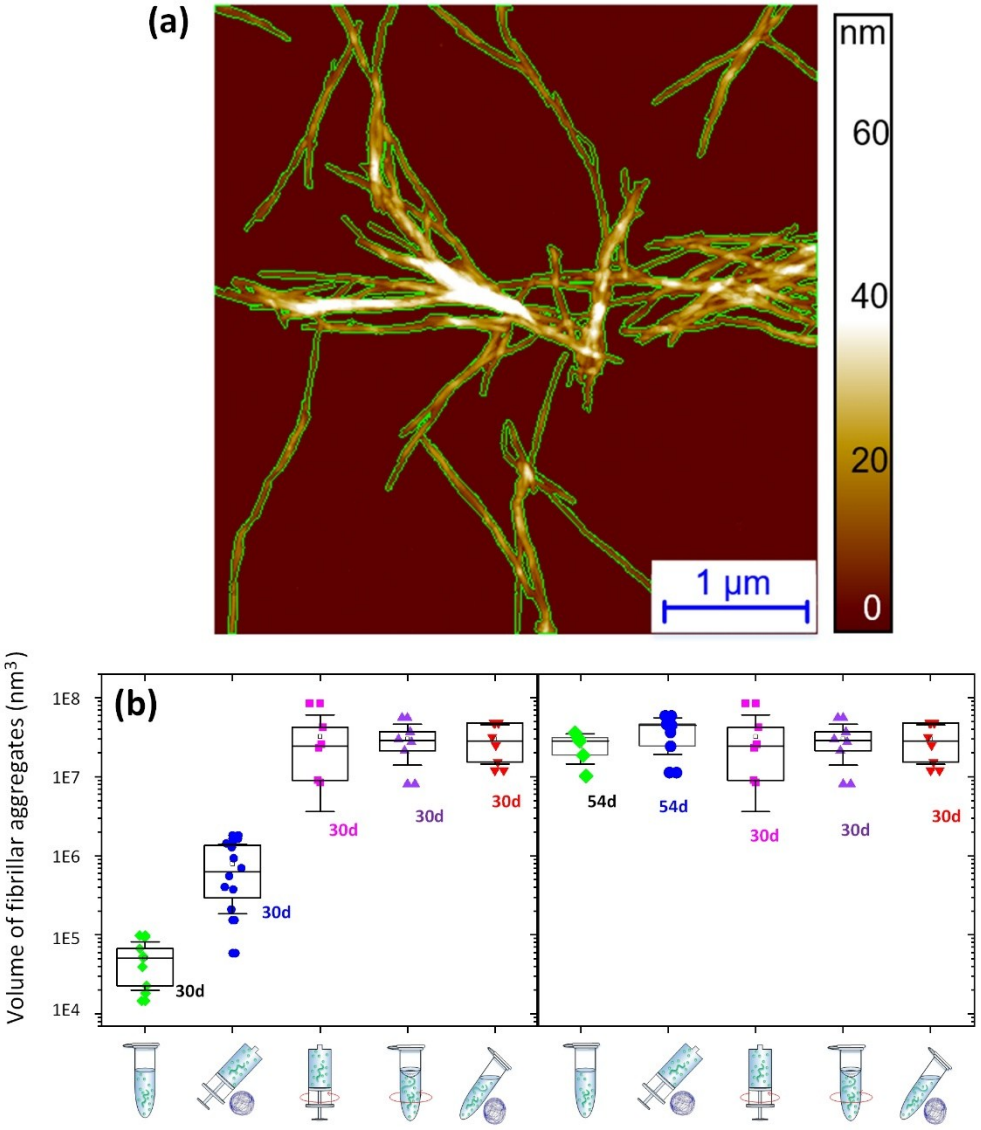

Figure S3| Method of fibril-volume characterization. The total volume of fibrillar aggregates was calculated on the $4 \times 4\ \mu m^2$ on six random-located AFM images from different locations on the mica surface were collected and analyzed in each condition. (b) A statistical data of the volume of fibrillar aggregates obtained at the same time point after 30-days incubation (left) and of the mature fibrils obtained in the plateau phase of aggregation. It is clear that, after 30-d incubation, the fibrillar aggregates formed in the Static-Epp and microgravity-Syr conditions were two orders lower than that of other conditions. In comparison, these values of mature fibrils in each condition are in the same order of magnitude, indicating that the initiating monomeric protein could yield the similar amount of fibrillar aggregates in the final plateau stage under different studied conditions.

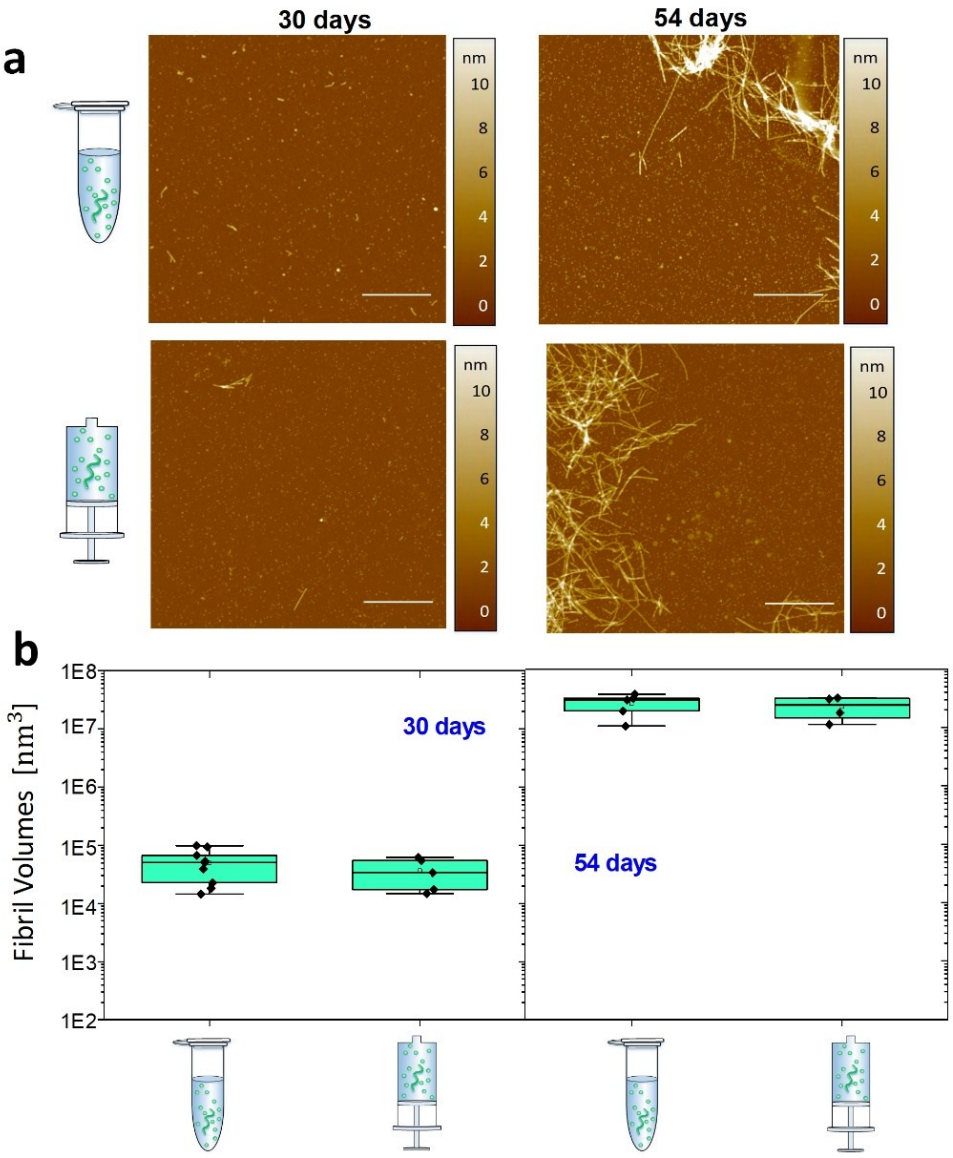

Figure S4| Comparison of amyloid formation in static conditions in Eppendorf tubes with an air-water interface and syringes without an air-water interface. (a) AFM images of protein aggregates obtained in Static-Epp and Static-Syr conditions after 30 and 54 days of incubation. The scale bar is 1 µm. (b) Statistical analysis of the volume of the formed fibrillar aggregates after 30 days (left) and 54 days (right) of static incubation for Eppendorf and syringe incubation. This result indicates that a similar speed of fibrillar aggregates formation in these two conditions.

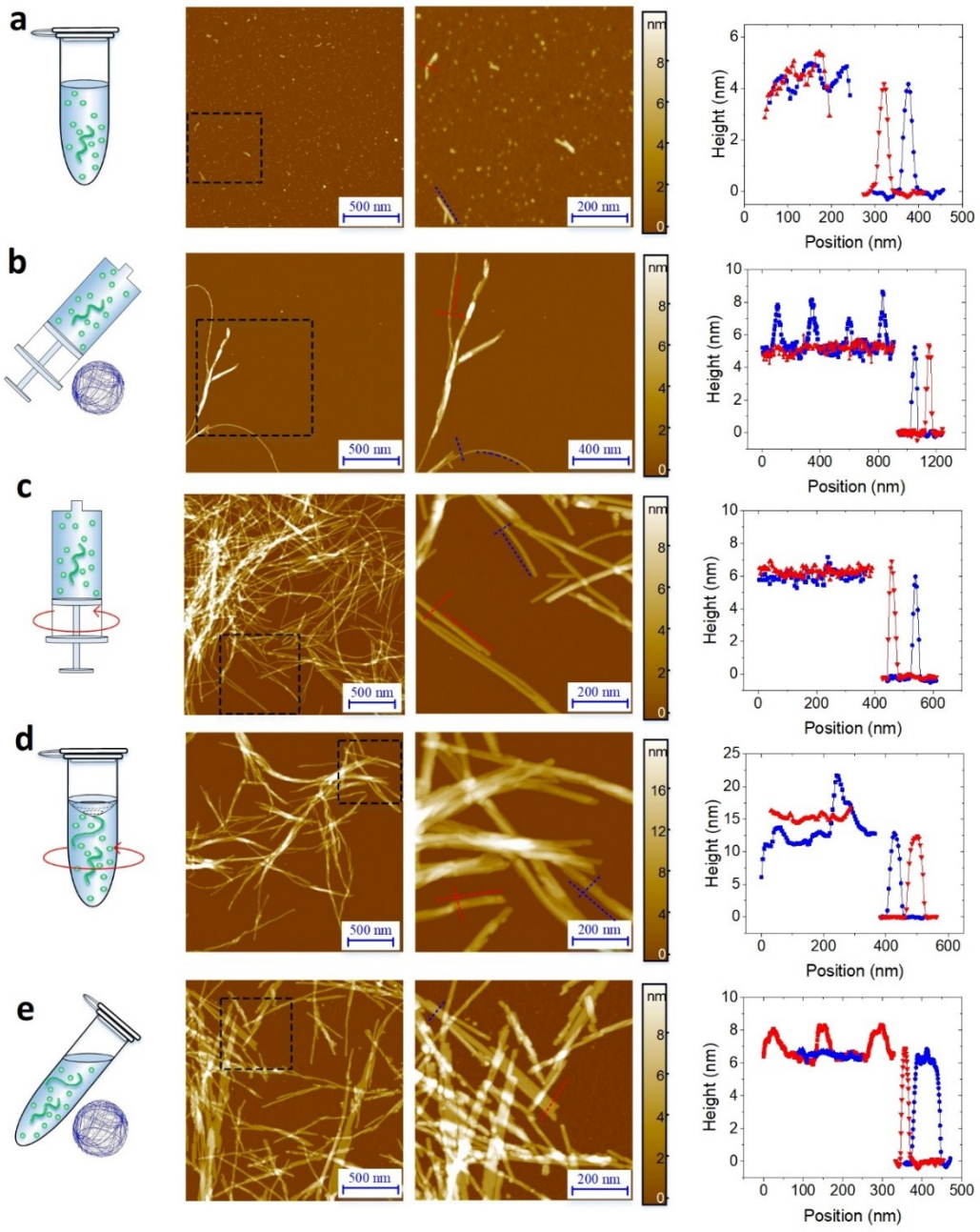

Figure S5| Morphological characterization of amyloid fibrils after 30 days of incubation. (Left) AFM images of fibrils formed after 30 days. (Middle) The zoom-in AFM image in the area indicated in (a1-e1) to show the detailed shape of fibrils. (Right) The fibril height profiles along the dashed lines indicated in the AFM images.

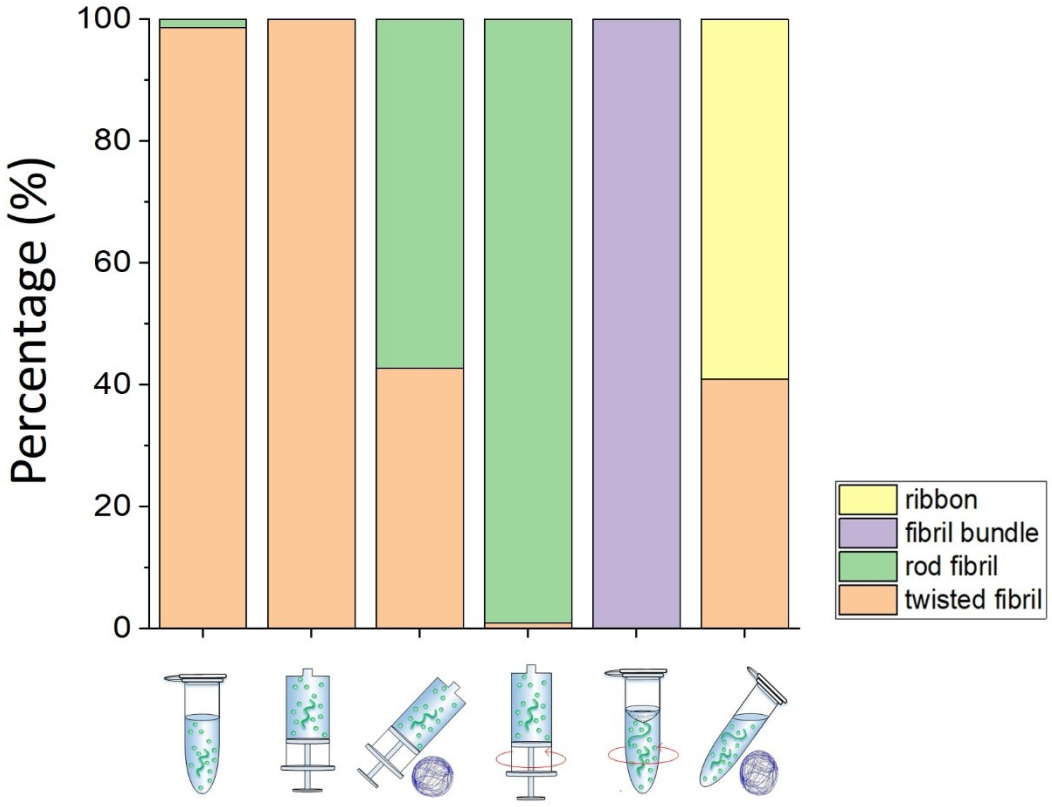

Figure S6| Polymorphism of mature amyloid fibrils produced in each condition. Statistical analysis of fibril morphology in each condition. The result shows that the dominating twisted fibrils was found in the static conditions, while homogeneous rod fibrils and fibril bundles were observed in the OShaking-Syr and OShaking-Epp conditions respectively. However, heterogeneous fibrils, including rod fibril and twisted fibril, were revealed in the microgravity-Syr condition, and the coexistence of ribbon and twisted fibril was observed from the microgravity-Epp condition. In each condition, we measured more than 60 fibrils.

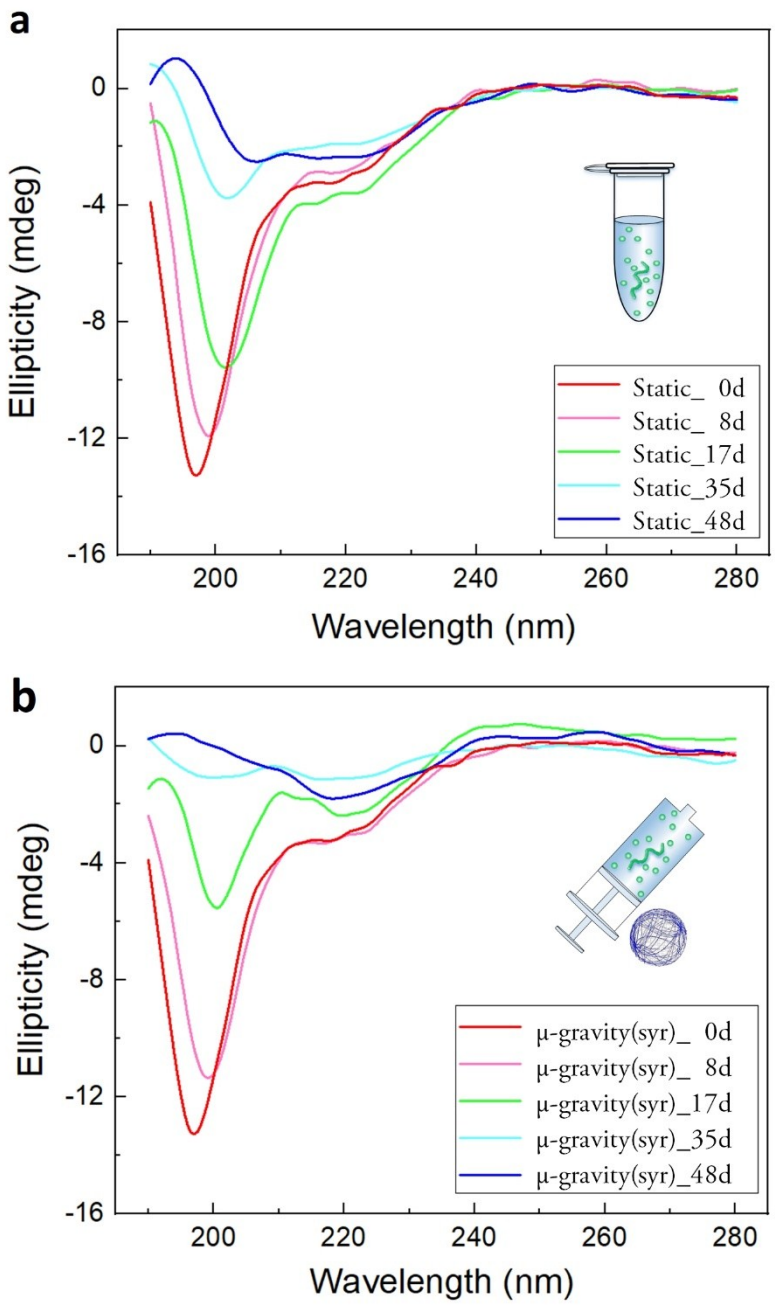

Figure S7| CD spectra of α-Synuclein solution in Static-Epp (a) and microgravity-Syr (b) conditions until 48 days of incubation. The spectra of both conditions show a steady and slow shrinking of the absorption dip at 198 nm, referring the gradual decrease of helical conformation in the solution, until its appearance after 48 days of incubation.

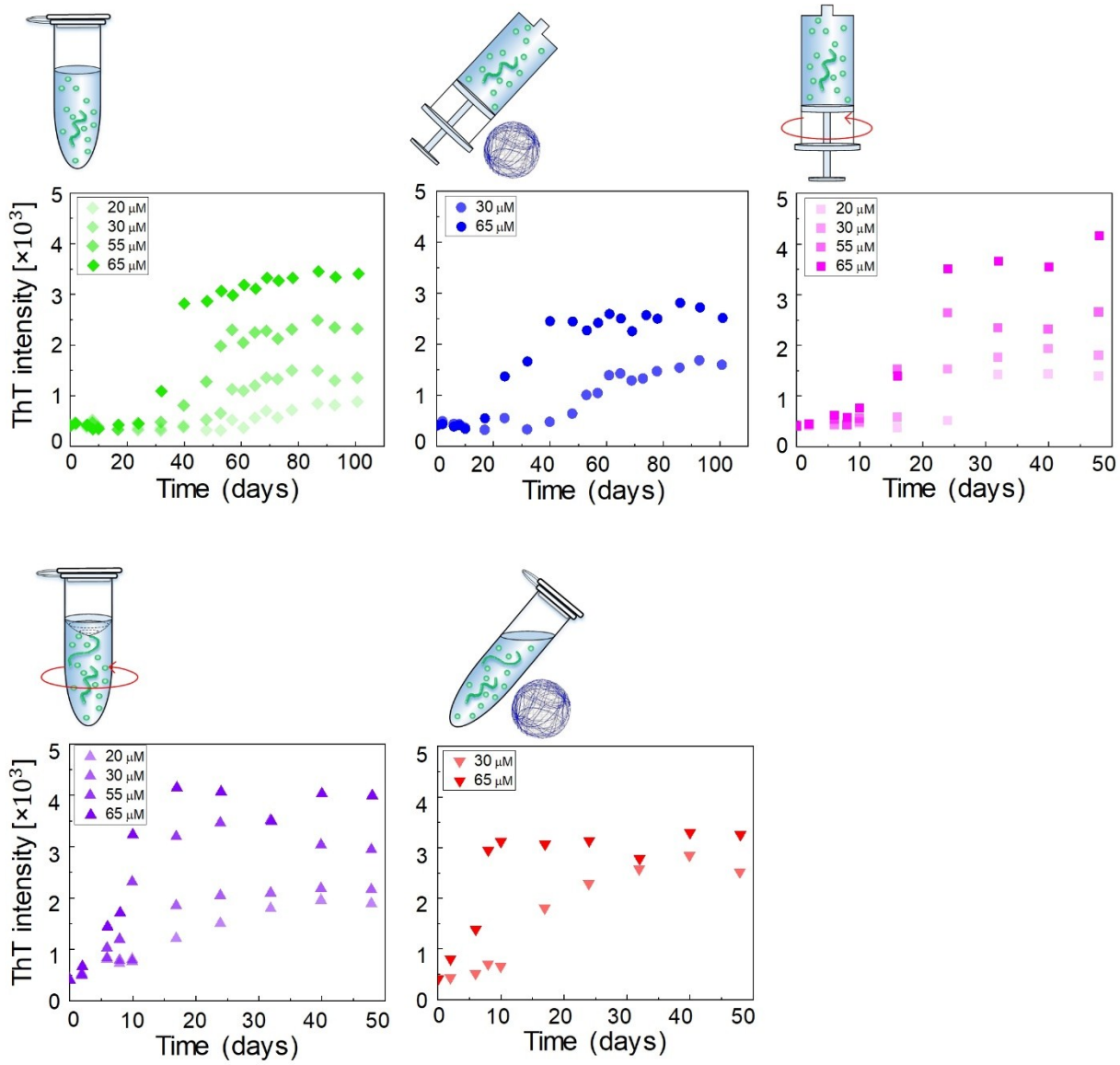

Figure S8| ThT assay of α-synuclein at different concentrations in each condition. The ThT fluorescence measurement of α-Synuclein of monomeric protein concentration of 20, 30, 55, 65 μM in the static-Epp, OShaking-Syr, OSaking-Epp conditions. Another two assays were performed of initiating protein concentration of 30 and 65 μM in the microgravity-Syr and microgravity-Epp conditions. Only two measurements were performed in the microgravity condition due to the limited space on the rotating plate of the RPM system, since placing the sample away from the rotational center, would not allow to have average low gravity vector during the experiment[3,4].

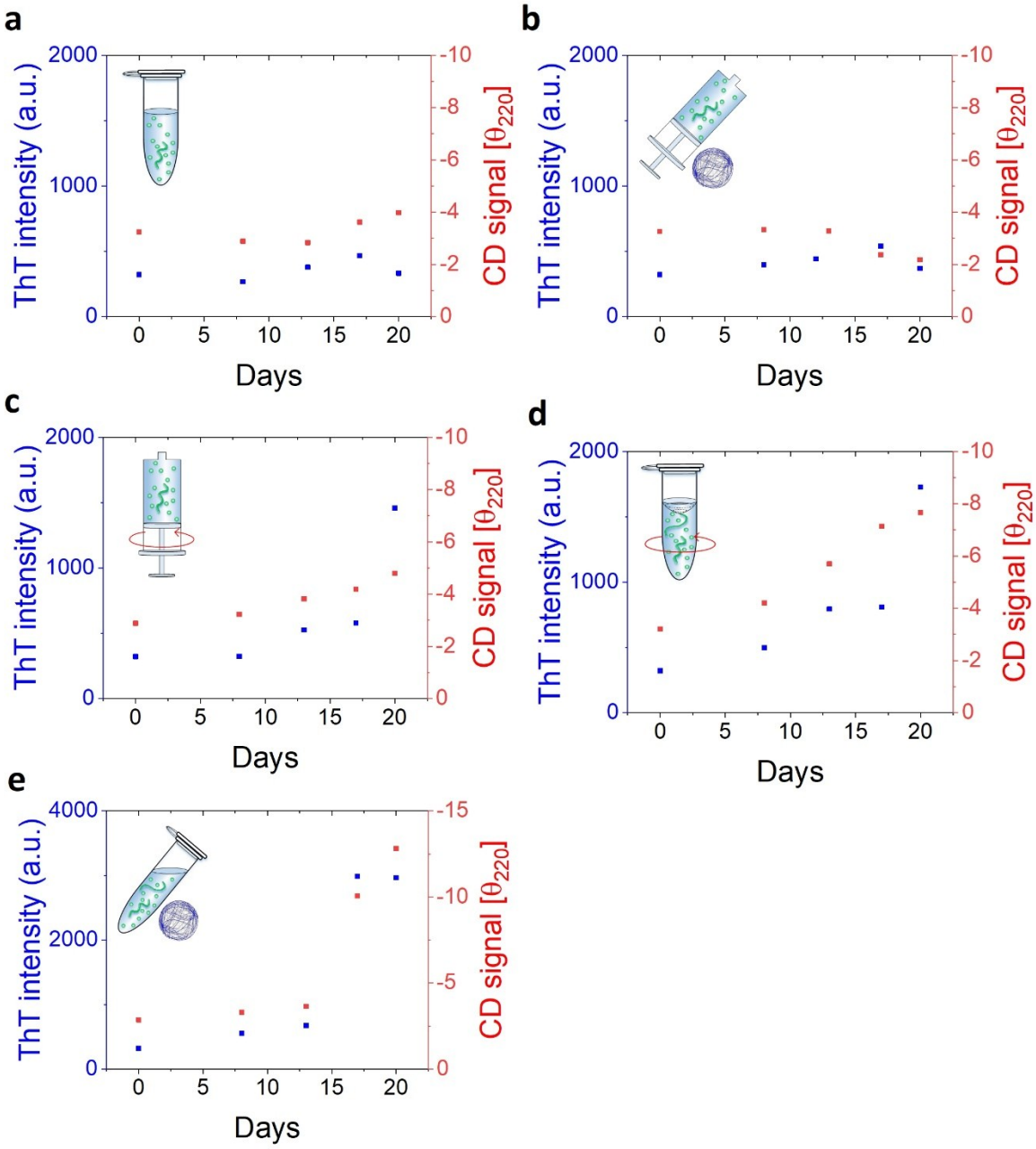

Figure S9| Correlation of ThT assay and CD spectroscopy at 45 µM. (a-e) ThT fluorescence intensity and the CD signal on the spectrum at 220 nm of the protein solution at the initial protein concentration of 45 µM at the same time point were plotted as a function of incubation time under different studied conditions.

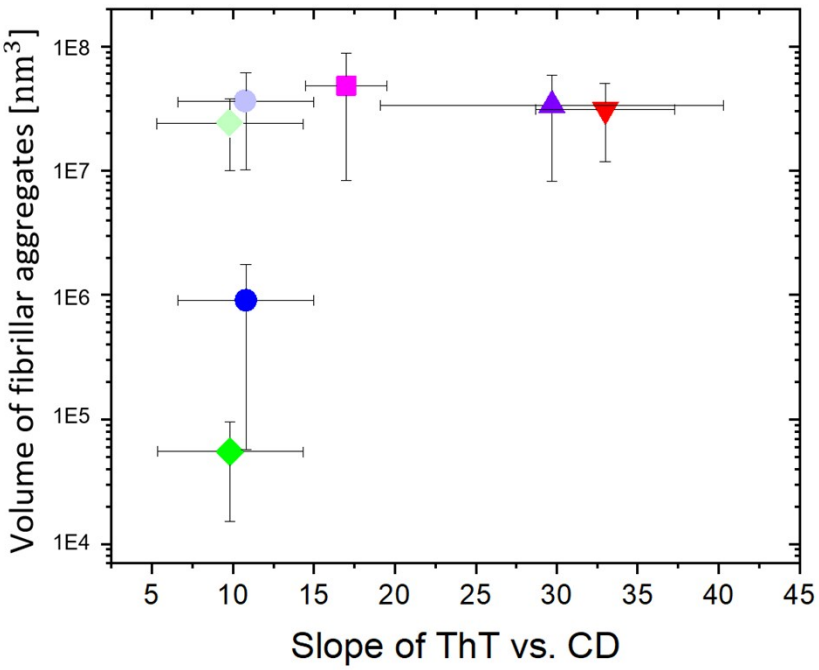

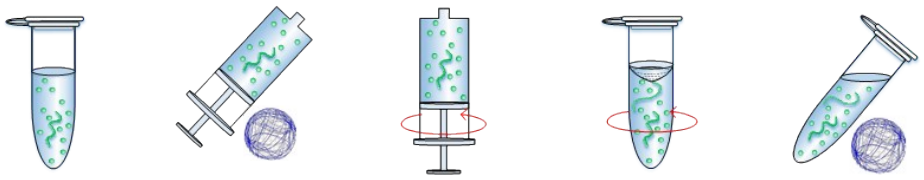

Fibril volume (10^7 nm^3)	**0.0032±0.0021**	**0.094±0.055**	**2.4±1.6**	**2.8±0.7**	**2.9±1.3**
Slop of ThT/CD signal	**8.8±4.5**	**10.8±4.2**	**17±2.5**	**29.7±10.6**	**33±4.3**

Figure S10| The comparison between fibril volume and the slope of CD/ThT measurement. Upper: The plot shows that the volume of fibrillar aggregates formed under incubation in each condition after 30 days (solid points) and 54 days (transparent points), against the slope of CD vs. ThT measurement. Bottom: The AFM quantified volumes of formed amyloid fibrils after 30 days, and the correlation value of spectroscopic and kinetic data. These data show that the trends of aggregation process characterized with different approaches were in good agreement.

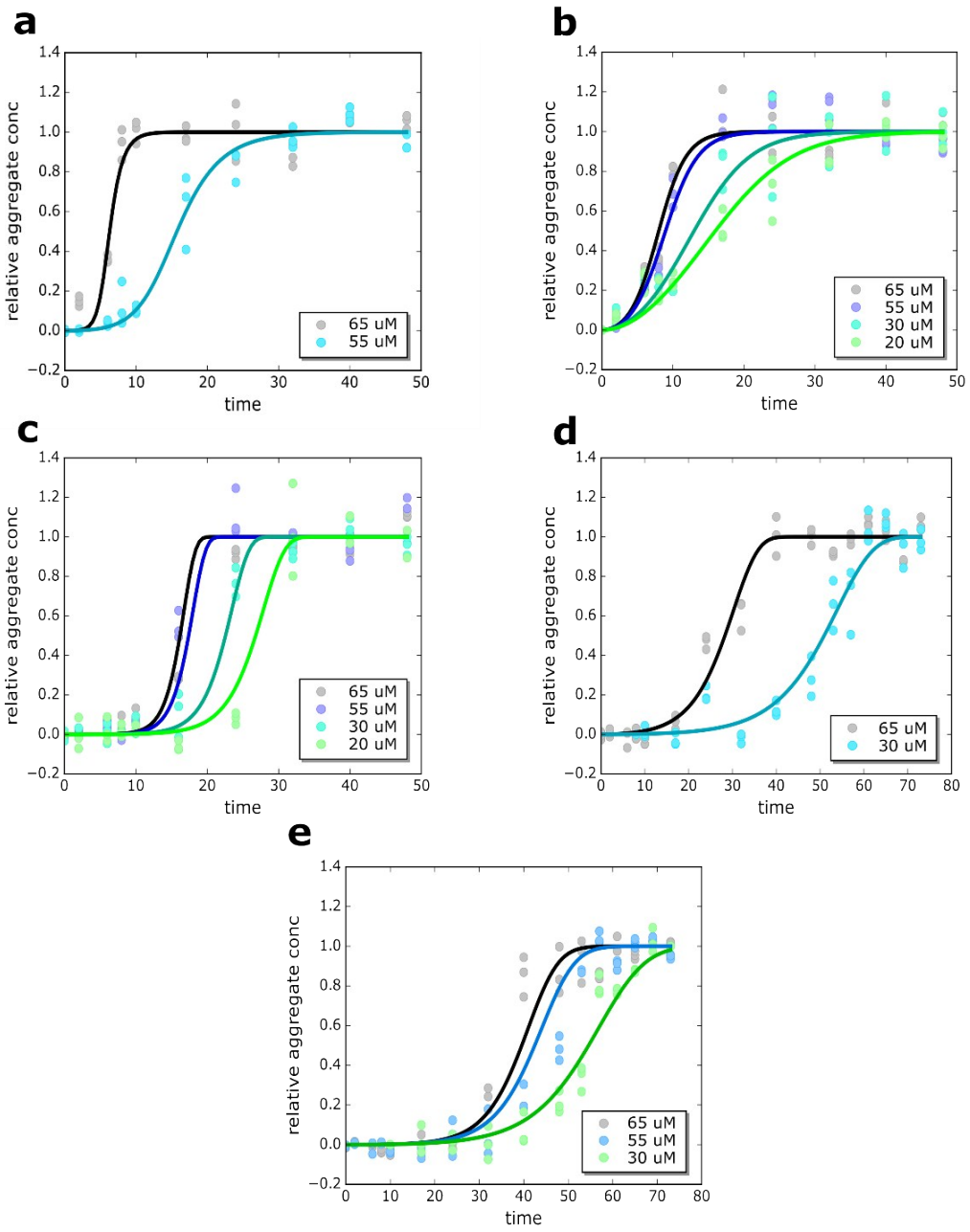

Figure S11| Global fitting of the ThT aggregation assays. The kinetic data obtained in ThT assays was fitted to an integrated rate law describing the aggregation kinetics. Global fits were performed separately for each experimental condition, i.e. the fitted parameters were the same for all concentrations recorded at one set of conditions, but were allowed to differ for different conditions. The parameters obtained from these fits are shown in the main text Figure 4e. Shown here are the overlay of best fits (solid lines) on data (points) for a) microgravity-Epp b) OShaking-Epp c) OShaking-Syr d) microgravity-Syr and e) Static-Epp experimental conditions.

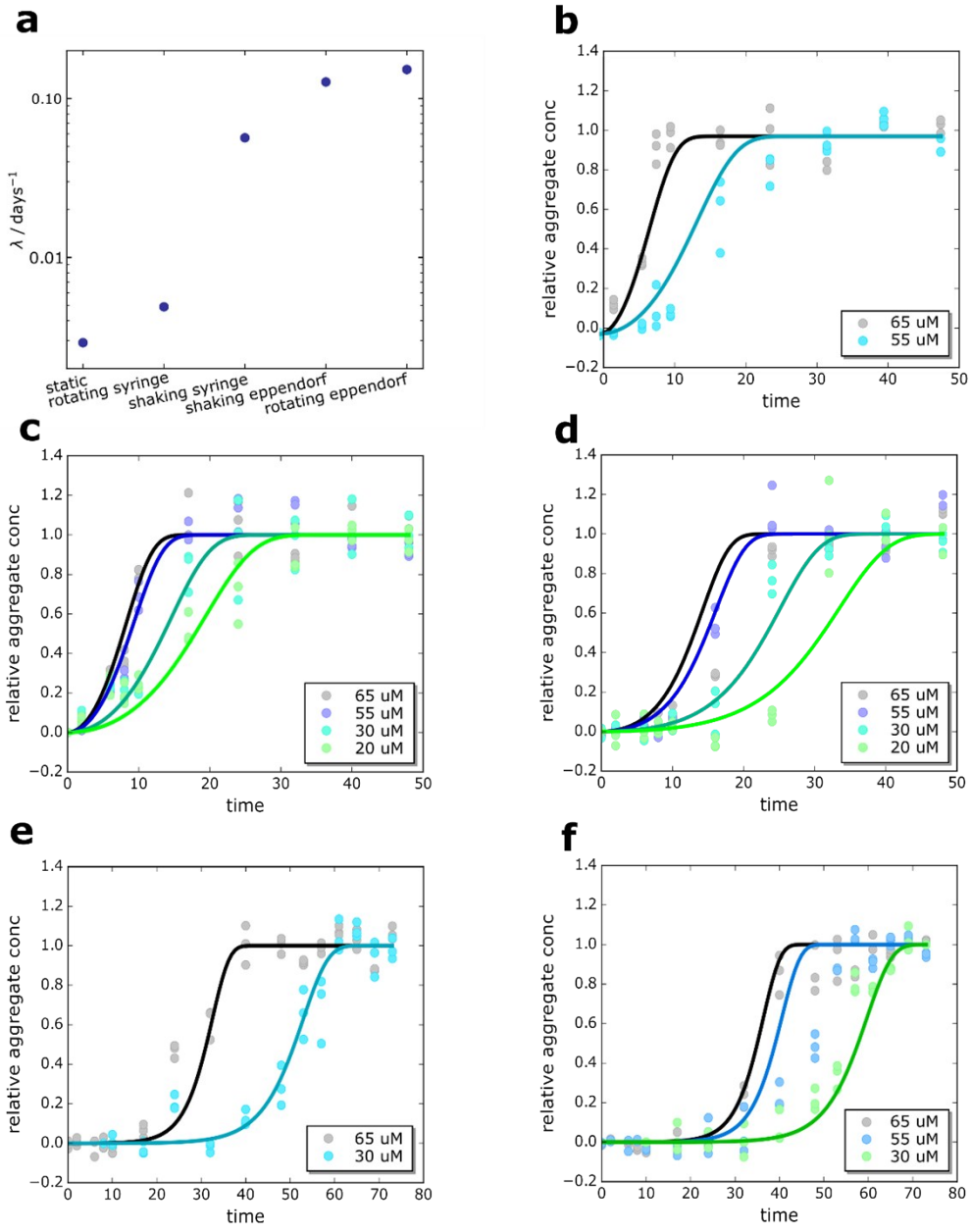

Figure S12| Global fitting results assuming that the tested experimental conditions mainly affected primary nucleation of α-synuclein aggregation: The rate of primary nucleation was allowed to vary with the experimental conditions, whereas the remaining fitting parameters were constrained to one global value for all conditions. All curves of the ThT assays were fitted simultaneously, but they are plotted separately for each condition to improve clarity. a) Rate of primary nucleation against tested experimental conditions. b) – f) Overlay of best fit (solid line) on data (points) for b) microgravity-Epp c) OShaking-Epp d) OShaking-Syr e) microgravity-Syr and f) Static-Epp experimental conditions.

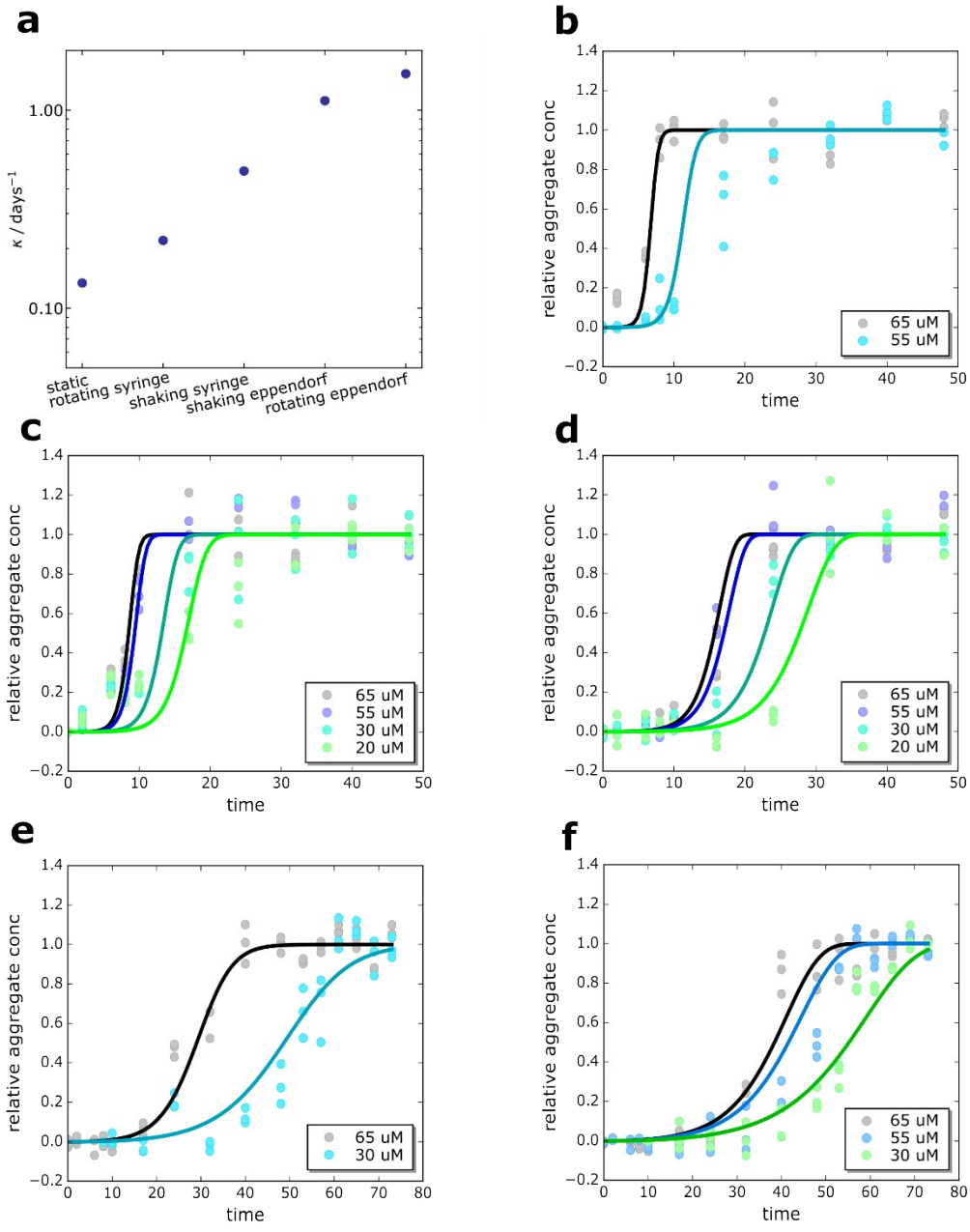

Figure S13| Global fitting results assuming that the tested experimental conditions mainly affected secondary processes of α-synuclein aggregation: The rate of the secondary process was allowed to vary with the experimental conditions, whereas the remaining fitting parameters were constrained to one global value for all conditions. All curves of the ThT assays were fitted simultaneously, but they are plotted separately for each condition to improve clarity. a) Rate of secondary processes against tested experimental conditions. b) – f) Overlay of best fit (solid line) on data (points) for b) microgravity-Epp c) OShaking-Epp d) OShaking-Syr e) microgravity-Syr and f) Static-Epp experimental conditions.

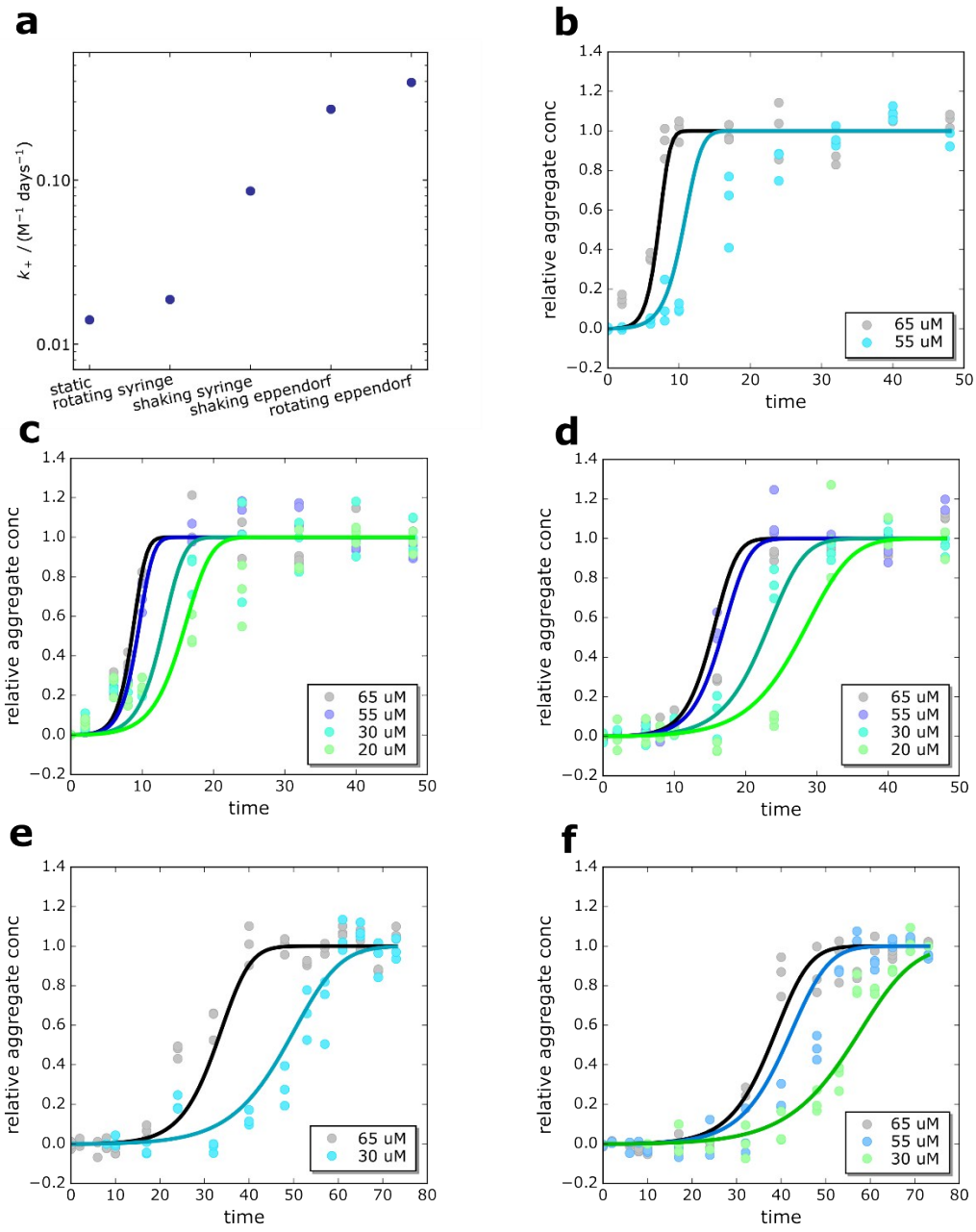

Figure S14| Global fitting results assuming that the tested experimental conditions mainly affected elongation of α-Synuclein aggregation: The rate of elongation was allowed to vary with the experimental conditions, whereas the remaining fitting parameters were constrained to one global value for all conditions. All curves of the ThT assays were fitted simultaneously, but they are plotted separately for each condition to improve clarity. a) Rate constant of elongation against tested experimental conditions. b) – f) Overlay of best fit (solid line) on data (points) for b) microgravity-Epp c) OShaking-Epp d) OShaking-Syr e) microgravity-Syr and f) Static-Epp experimental conditions.

Supplementary Reference

1. Ruggeri, F. S. *et al.* Influence of the β-Sheet Content on the Mechanical Properties of Aggregates during Amyloid Fibrillization. *Angewandte Chemie* **127**, 2492–2496 (2015).
2. Ruggeri, F. S., Šneideris, T., Vendruscolo, M. & Knowles, T. P. J. Atomic force microscopy for single molecule characterisation of protein aggregation. *Archives of Biochemistry and Biophysics* **664**, 134–148 (2019).
3. Dinarelli, S. *et al.* Erythrocyte's aging in microgravity highlights how environmental stimuli shape metabolism and morphology. *Sci Rep* **8**, 1–12 (2018).
4. van Loon, J. J. W. A. Some history and use of the random positioning machine, RPM, in gravity related research. *Advances in Space Research* **39**, 1161–1165 (2007).